

Articles

Synthesis, Biological Evaluation, and Binding Mode of Novel 1-[2-(Diarylmethoxy)ethyl]-2-methyl-5-nitroimidazoles Targeted at the HIV-1 Reverse Transcriptase

Romano Silvestri,[†] Marino Artico,^{*,†} Gabriella De Martino,[†] Rino Ragno,[‡] Silvio Massa,[§] Roberta Loddo,^{||} Chiara Murgioni,^{||} Anna Giulia Loi,[⊥] Paolo La Colla,^{*,||} and Alessandra Pani^{||}

Istituto Pasteur–Fondazione Cenci Bolognetti, Dipartimento di Studi Farmaceutici, Università di Roma “La Sapienza”, BOX 36, Roma 62, P.le Aldo Moro 5, I-00185 Roma, Italy, Dipartimento di Studi di Chimica e Tecnologia delle Sostanze Biologicamente Attive, Università di Roma “La Sapienza”, P.le Aldo Moro 5, I-00185 Roma, Italy, Dipartimento Farmaco Chimico Tecnologico, Università di Siena, via Aldo Moro, I-53100 Siena, Italy, Novirio Pharmaceuticals, Inc., Boston, and Dipartimento di Biologia Sperimentale, Sezione di Microbiologia, Università degli Studi di Cagliari, Cittadella Universitaria, SS 554 Km 4.500, I-09042 Monserrato, Cagliari, Italy

Received April 18, 2001

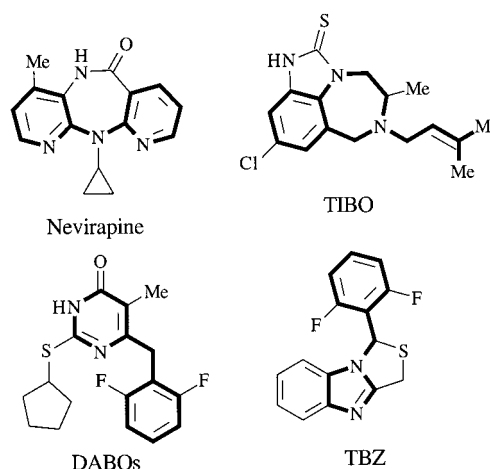
A novel series of 1-[2-(diarylmethoxy)ethyl]-2-methyl-5-nitroimidazole (DAMNI) analogues were synthesized and tested in cell-based assays and in enzyme assays against HIV-1 recombinant reverse transcriptase (RT). Preparation of the new derivatives was performed by reacting the appropriate benzhydrols or the corresponding bromides with 1-(2-hydroxyethyl)-2-methyl-5-nitroimidazole or the 3-hydroxypropyl homologue. Several compounds showed anti-HIV-1 activity in the submicromolar range. Structure–activity relationship studies suggested that meta substitution at one phenyl ring of the diarylmethane moiety strongly influences the antiviral activity. The 3,5-disubstitution at the same phenyl ring led to less potent derivatives. Molecular modeling and docking studies within the RT non-nucleoside binding site confirmed that DAMNIs, similar to other NNRTIs such as TNK-651 and delavirdine (BHAP U90152), assume a butterfly-like conformation that appears to be halfway between that of classical NNRTIs, such as nevirapine, HEPT, TBZ, TIBO, and DABOs, and the conformation of BHAPs. In particular, the diphenylmethane moiety mimics the wings whereas the 1-(2-methyl-5-nitroimidazolyl)ethane portion resembles the BHAP 5-methanesulfonamidoindole-2-carboxylpiperazine portion.

Introduction

On the basis of molecular modeling and X-ray structure investigations on nevirapine and TIBO, Schäfer et al.^{1,2} proposed a three-dimensional (3D) model describing the structural elements that they thought were determinant for anti-HIV-1 activity: (i) two π systems (normally a benzene ring and an extended π system) arranged in a “butterfly-like orientation”; (ii) an additional lipophilic region between them, such as a carbonyl or thiocarbonyl group near the benzene ring; (iii) a methyl group in the extended π system.

Other agents, such as DABOs,³ α -APA,⁴ and TBZ,⁵ are examples of agents conformationally related to nevirapine and TIBO (Chart 1). They were found to potently inhibit HIV-1 reverse transcriptase (RT) and were classified among the “butterfly-like” congeners.

Chart 1



Because the anti-HIV-1 activity of these compounds seems to be strongly related to the reproduction of the structural elements described in the Schäfer 3D model, we undertook synthetic studies to develop novel anti-HIV-1 agents having the diarylmethane unit as a “butterfly-like” conformational moiety.

* To whom correspondence should be addressed. For M.A.: fax, +39 06 4462731; e-mail, marino.artico@uniroma1.it. For P.L.C.: fax, +39 070 6754148; e-mail, placolla@unica.it.

[†] Dipartimento di Studi Farmaceutici, Università di Roma “La Sapienza”.

[‡] Dipartimento di Studi di Chimica e Tecnologia delle Sostanze Biologicamente Attive, Università di Roma “La Sapienza”.

[§] Università di Siena.

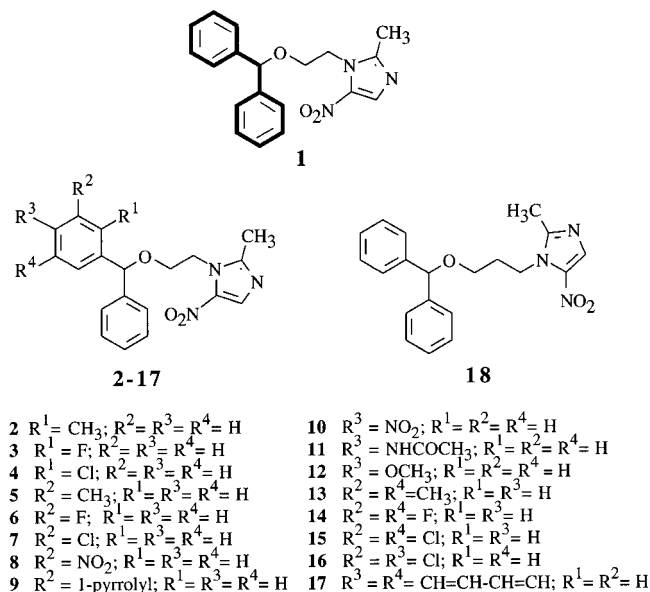
^{||} Università di Cagliari.

[⊥] Novirio Pharmaceuticals, Inc..

This approach soon led to the discovery of 1-[2-(diarylmethoxy)ethyl]-2-methyl-5-nitroimidazoles, named with the acronym DAMNIs, a novel family of non-nucleoside reverse transcriptase inhibitors (NNRTIs) active at submicromolar concentrations.⁶

Among the first series of DAMNIs, the parent compound **1** (Chart 2) emerged as a potent inhibitor of

Chart 2

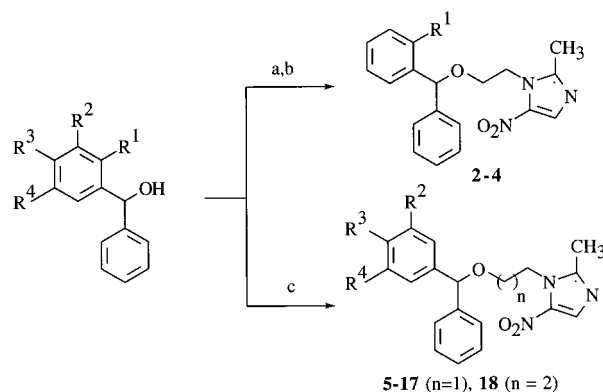


HIV-1 growth and was selected as a lead compound for further improvements. Furthermore, a preliminary structure-activity relationships (SAR) study showed that both nitro and methyl substituents bound to the imidazole ring were highly positive for anti-HIV-1 activity. In contrast, introduction of a set of either electron-withdrawing or electron-donating groups in the para position of one phenyl ring of the diarylmethyl moiety was detrimental for antiretroviral activity.

These findings prompted us to prepare a new series of DAMNIs (compounds **2–18**) for evaluating the influence on antiviral activity of (i) ortho and meta mono-substitution at one phenyl ring, (ii) substituents at the para position different from methyl or halogens, (iii) disubstitution at position 3 and 5 of a phenyl ring; (iv) replacement of one phenyl with the bulkier naphthyl ring; (v) elongation of the oxyethyl chain connecting the diarylmethyl moiety to the imidazole ring.

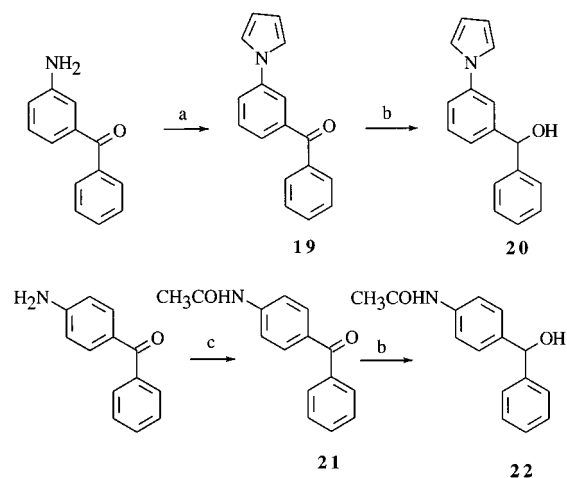
All the new compounds were evaluated for their cytotoxicity and anti-HIV-1 activity in MT-4 cells, and some of them were assayed against highly purified recombinant wild-type HIV-1 RT using homopolymeric template primers. The results of assays were expressed as cytotoxicity (CC₅₀), anti-HIV-1 activity (EC₅₀), selectivity (SI given as the CC₅₀/EC₅₀ ratio), and RT inhibitory activity (IC₅₀). Qualitative and quantitative SAR studies were performed, and the binding mode of DAMNIs into the non-nucleoside binding site (NNBS) of HIV-1 RT was investigated by molecular modeling. Evaluation of antiretroviral activity of selected DAMNIs (**2–8**) against strains carrying the clinically relevant RT mutations K103N, Y181C, and the double mutant K103N–Y181C was also performed.

Scheme 1^a



^a (a) PBr₃, diethyl ether, RT, 4h; (b) 1-(2-hydroxyethyl)-2-methyl-5-nitroimidazole, K₂CO₃, acetone, reflux, 7 days; (c) 1-(2-hydroxyethyl)-2-methyl-5-nitroimidazole, 1-(3-hydroxypropyl)-2-methyl-5-nitroimidazole for **18**, PTSA, benzene, reflux, 4 h, Dean–Stark trap.

Scheme 2^a



^a (a) 2,5-Dimethoxytetrahydrofuran, reflux, 1 h; (b) NaBH₄, THF/H₂O, reflux, 2 h; (c) CH₃COCl, pyridine, RT, 3 h.

Chemistry

Derivatives **2–4** were synthesized by heating the appropriate diarylbromomethanes with 1-(2-hydroxyethyl)-2-methyl-5-nitroimidazole in the presence of potassium carbonate. The required diarylbromomethanes were obtained by reacting the precursors benzhydrols with phosphorus tribromide. Derivatives **5–18** were prepared by refluxing the benzhydrols with 1-(2-hydroxyethyl)-2-methyl-5-nitroimidazole (**5–17**) or 1-(3-hydroxypropyl)-2-methyl-5-nitroimidazole⁷ (**18**) in the presence of *p*-toluenesulfonic acid (PTSA) with azeotropic removal of water by a Dean–Stark trap (Scheme 1).

Benzhydrols **20** and **22** were prepared by NaBH₄ reduction of the corresponding ketones **19** and **21**, which, in turn, were obtained by reacting 3-aminobenzophenone⁸ with 2,5-dimethoxytetrahydrofuran according to the Clauson–Kaas⁹ procedure or by acetylation of 4-aminobenzophenone¹⁰ with acetyl chloride in pyridine, respectively (Scheme 2).

SAR Evaluation

To discover novel DAMNI analogues with greater potency and selectivity, we extended our SAR studies

to assess the effect of a variety of substituents bound to the ortho, meta, and para positions of one phenyl ring. In the first series of DAMNIs, we had found that the introduction of methyl, chloro, and fluoro at the para position of one phenyl ring of the diarylmethane moiety of **1** gave compounds with decreased antiviral activity.⁶ In the present work, therefore, we decided to explore the anti-HIV activity of ortho- and meta-substituted counterparts.

As a rule, meta-substituted compounds showed high antiviral activity and, being devoid of cytotoxicity, they also shared high selectivity indexes. Compounds bearing meta-fluoro or meta-methyl substituents (SI >2000) were the most selective analogues, followed, in decreasing order of potency, by the meta-chloro (SI >1000) derivative. The related ortho derivatives were more cytotoxic and less potent. Substituents, such as nitro and 1*H*-pyrrolyl, introduced at the meta position, did not improve the anti-HIV-1 activity of DAMNI analogues.

Some para-phenyl derivatives bearing substituents different from methyl and halogens were also synthesized, but the results of anti-HIV-1 assays confirmed the reduced activity of para-substituted analogues (see derivatives **10–12**).

The above results suggest that meta monosubstitution correlates with the antiviral activity better than the ortho- and para-monosubstitutions and that fluorine is the substituent conferring the highest potency and selectivity of the series. This feature needs to be carefully considered in the design of novel DAMNIs.

The encouraging results obtained with meta-monosubstituted derivatives, and the high anti-HIV-1 activity shown by some dimethylphenyl and dihalophenyl NNRTIs such as DABOs,³ α -APA,⁴ TBZ,⁵ HEPT,¹¹ and the imidazole derivative AG 1549,¹² prompted us to prepare some disubstituted DAMNIs. In general, disubstitution gave derivatives with cytotoxicities and antiviral activities comparable to those of monosubstituted counterparts. However, unlike monosubstituted compounds, the 3,5-dimethyl and 3,5-difluoro derivatives were significantly more potent than the 3,5-dichloro counterpart.

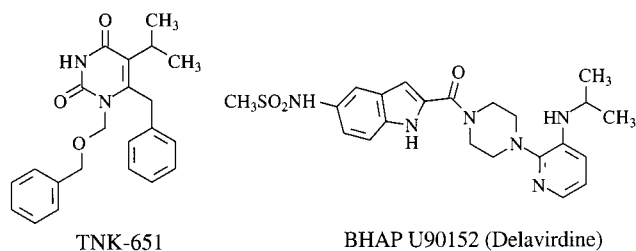
It is noteworthy that replacement of a phenyl group by a 2-naphthyl ring (compound **17**) resulted in significant loss of activity. Analogously, the lengthening of the alkyl chain connecting the diphenylmethoxy group to the 2-methyl-5-nitroimidazole (compare **1** with **18**) resulted in a net decrease of both cytotoxicity and antiviral activity.

When tested against K103N, Y181C, and the double mutant K103N–Y181C, none of the test compounds (**2–8**), the lead compound **1** included, were active in cell-based assays (data not shown).

Molecular Modeling of DAMNIs

Docking and Binding Mode Analysis. Although DAMNIs are chemically dissimilar from the other classes of NNRTI, some of their molecular structural features can be related to the general NNRTI mode of binding within the RT NNBS. In fact, the diphenylmethyl group could represent the two π systems of Schäfer's butterfly 3D model, and the 2-methyl-5-nitroimidazolyl moiety could occupy the same NNBS portion filled by either the *N*₁-phenylmethoxymethyl substituent of TNK-651¹³ or the 5-methanesulfonami-

Chart 3



doindole-2-carboxypiperazinyl portion of BHAP U-90152 (delavirdine)^{14,15} (Chart 3), thus making favorable interactions with the surroundings residues LYS104, VAL106, PRO225, PHE227, LEU234, PRO236, and TYR318 (Figure 1).

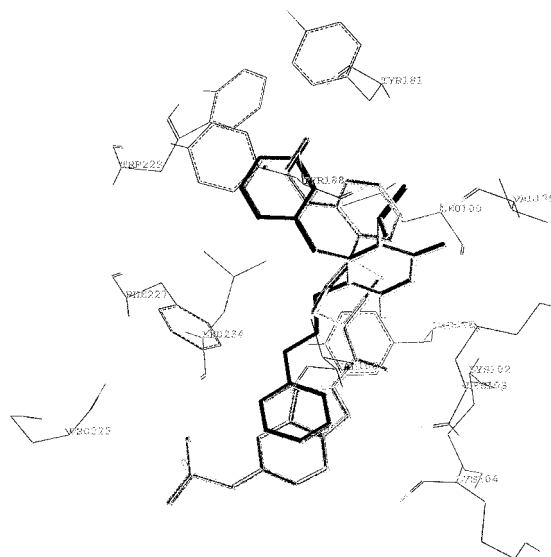


Figure 1. TNK-651 and delavirdine within the HIV-1 RT NNBS.

Starting from these observations and using compound **1** as a lead, the binding mode of DAMNI was explored, first aligning **1** to TNK-651 and then placing it into the NNBS. Docking experiments have been used to refine the binding geometry of the new HIV-RT/1 complex. Finally, by the application of the VALIDATE II method,^{16–18} a quantitative evaluation of the docking was performed.

Compound **1** was selected as a representative member for the DAMNIs because of the absence of any chiral atom and the higher activity shown as a RT inhibitor among the first series of DAMNIs. Conformational studies were carried out by MACROMODEL 6.5 using the bound conformation obtained by a docking experiment of **1** (SYBYL/FLEXIDOCK) inside the NNBS.

The coordinates of HIV-1 RT/TNK-651 taken from the Protein Brookhaven (PDB entry code 1rt2) database complex were initially used as a template to model **1**. A field-fit procedure using the atomic charges from the Gasteiger–Hückel molecular mechanic method was undertaken to align **1** to the reference compound TNK-651. The same alignment procedure with delavirdine (pdb entry code 1klm) as a reference compound led to a second starting alignment. Along with the field-fit procedure, two other starting alignments were tried using the two global minimum conformations from GB/

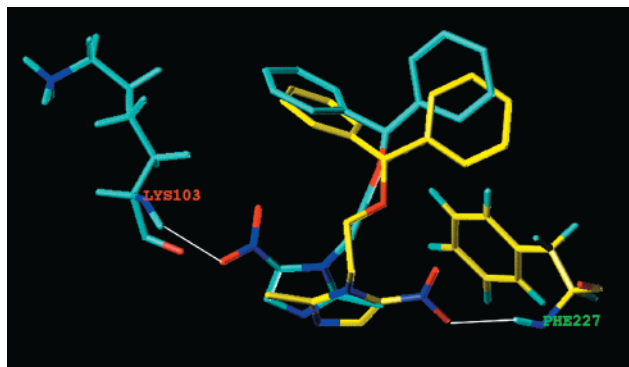


Figure 2. Binding mode of **1**: conformers a (yellow) and b (cyan). In white are the hydrogen bonds between the nitro group of DAMNI compound and the RT.

SA Monte Carlo analyses carried out on **1** (see below and the experimental procedure).

To explore the optimal binding geometry of **1** within the NNBS a SYBYL/FLEXIDOCK run was first used as previously reported.¹⁹ A Monte Carlo search was then undertaken to explore the conformational space of **1** inside the binding pocket, which was allowed to relax within 8 Å from the ligand's atoms, including a shell of 10 Å for electrostatic long-range interactions.

There is extensive experimental evidence for two possible binding conformations of **1** inside the NNBS (Figure 2). The two bound conformations are in good agreement with each other, and they differ only in the orientation of the 2-methyl-5-nitroimidazolyl moiety. In fact, one nitro-group oxygen forms a hydrogen bond with the hydrogen of the α -amino group of PHE227 (distance O \cdots H 2.59 Å, angle N–O \cdots H 104.1°, conformation a obtained from the SYBYL/FLEXIDOCK) or with that

of LYS104 (distance O \cdots H 2.53 Å, angle N–O \cdots H 116.4°, conformation b obtained from global minimum from the Monte Carlo search), depending on the orientation. To determine the most probable binding conformation, two further Monte Carlo searches on **1** alone were carried out, using as starting points the previously found binding conformations a and b. After 1000 MC steps in water (GB/SA method) two isoenergetic ($E_{\text{steric}} = -295.29$ kJ/mol) global minima were obtained, displaying a root-mean-square interatomic distance deviation (rmsd) value of 1.0383.

Inspection of the steric energies including the solvation term showed that, in water, conformation a ($E = -271.885$ kJ/mol) is definitively more stable than conformation b (-260.617 kJ/mol). Comparing the steric energies of the two binding modes with that of the global minima, the ligand strain energy (excluding the solvation term) of conformation b ($\Delta E_{\text{StrainEnergy}} = 75.641$ kJ/mol) was higher than that of conformation a ($\Delta E_{\text{StrainEnergy}} = 35.111$ kJ/mol). These values for the conformational energy penalties are higher than the value of 3 kcal/mol suggested by Boström,²⁰ although we are dealing with highly polar compounds (imidazoles bearing a nitro group), and some failures, due to the force field, must not be neglected as reported by Boström himself. Moreover, a direct comparison of the ligand–receptor interactions energies again revealed a better profile for conformation a.

In Table 2 are reported the electrostatic interaction energies (ESIE, Coulombic) and the steric interaction energies (SIE, van der Waals), which indicate that conformation a forms more stable contacts inside the NNBS than conformation b. Although multiple binding modes cannot be excluded, the above observations

Table 1. Cytotoxicity and Anti-HIV-1 Activity of DAMNI Derivatives **1–18**^a

compd	R ¹	R ²	R ³	R ⁴	n	CC ₅₀ ^b	EC ₅₀ ^c	SI ^d	IC ₅₀ ^e
2	CH ₃	H	H	H	1	76	0.2	380	0.2
3	F	H	H	H	1	63	0.2	315	0.4
4	Cl	H	H	H	1	52	0.6	85	0.6
5	H	CH ₃	H	H	1	>200	0.1	>2000	0.3
6	H	F	H	H	1	>200	0.1	>2000	0.5
7	H	Cl	H	H	1	>200	0.2	>1000	0.5
8	H	NO ₂	H	H	1	92.5	0.6	154	0.3
9	H	1-pyrryl	H	H	1	>200	14	>14	f
10	H	H	NO ₂	H	1	111	5	22	f
11	H	H	NHCOCH ₃	H	1	>200	>200	-	f
12	H	H	OCH ₃	H	1	>200	86	>2	f
13	H	CH ₃	H	CH ₃	1	200	0.4	>500	f
14	H	F	H	F	1	>200	1	>200	f
15	H	Cl	H	Cl	1	>200	45	>4	f
16	H	Cl	Cl	H	1	200	97	>2	f
17	H	H	CH=CH–CH=CH	H	1	>200	106	>1.8	f
18	H	H	H	H	2	96.5	35	3	f
18 ^g delavirdine ^h	H	H	H	H	1	>200 >30	0.2 0.01	>1000 >3000	0.05 1.1

^a Data represent mean values of at least two separate experiments. Variability among duplicate samples was lower than 15%. ^bCompound dose (μ M) required to reduce the viability of mock-infected cells by 50%, as determined by the MTT method. ^cCompound dose (μ M) required to achieve 50% protection of MT-4 cells from HIV-1 induced cytopathogenicity, as determined by the MTT method. ^dSelectivity index: CC₅₀:EC₅₀ ratio. ^eCompound dose required to inhibit the HIV-1 rRT activity by 50%. ^fNot determined. ^gReference 6. ^hMT-2 cells (ref 14).

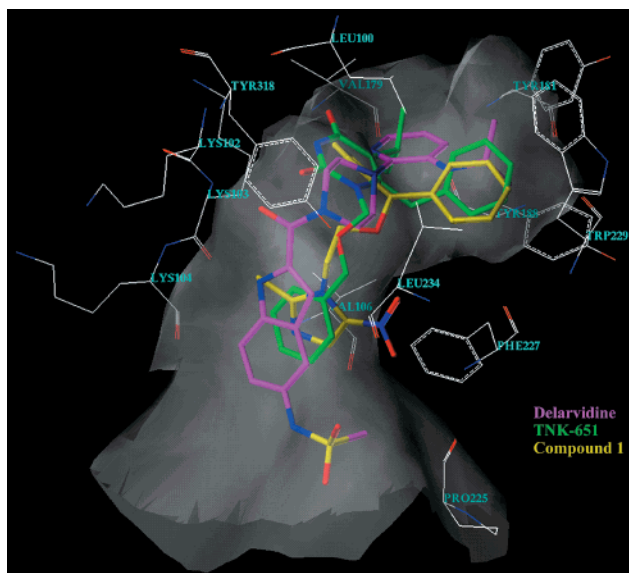


Figure 3. Binding mode of **1** compared to binding modes of TNK-651 and delarvidine.

Table 2. Energetics for Binding Conformations of **1**

conformation	ESIE ^a	SIE ^b	LSE ^c
a	-66.040	-221.788	35.111
b	-49.861	-184.704	75.641

^a ESIE: electrostatic interaction energies (kJ/mol). ^b SIE: steric interaction energies (kJ/mol). ^c LSE: ligand strain energy (kJ/mol).

strongly suggested adoption of conformation a as the probable binding mode for **1**.

The herein proposed binding mode for **1** (conformation a) is also quantitatively supported by the application of the VALIDATE II method, a variation of VALIDATE developed by Head et al.²¹ A hybrid QSAR/scoring function model specific for the NNRTI, obtained using 14 known RT inhibitors²² and eight selected parameters, was able to recalculate within a minimal error the experimental pIC₅₀ value of **1** (pIC₅₀^{exper} = 7.30, pIC₅₀^{pred} = 7.04); meanwhile, the HIV-RT/VALIDATE II model predicted the pIC₅₀ value for conformation b to be an order of magnitude lower than the experimental value.

Considering the multiple minima problem,²³ all the minima found from the Monte Carlo search inside the NNBS were submitted to the VALIDATE II procedure to search for alternative binding conformations. None of the predicted pIC₅₀ values calculated for all local minima conformations found reproduced the experimental value of **1** better than that calculated for conformation a.

Inspection of conformation a inside the NNBS (Figure 3) led to the following conclusions: (i) one phenyl ring of **1** makes favorable π - π interactions with the hydrophobic pocket formed by the side chains of TYR181, TYR188, PHE227, TRP229, and LEU234; (ii) the other phenyl group of **1** occupies a more lipophilic pocket formed by the side chains of LEU100, LYS103, VAL106, VAL179, and GLY190; (iii) the ethane bridge interacts in part with the side chain termini of VAL106, LEU234, and TYR318; (iv) 2-methyl-5-nitroimidazolyl moiety, the more hydrophilic portion of **1**, binds to the least hydrophobic section of NNBS, exerting favorable contacts

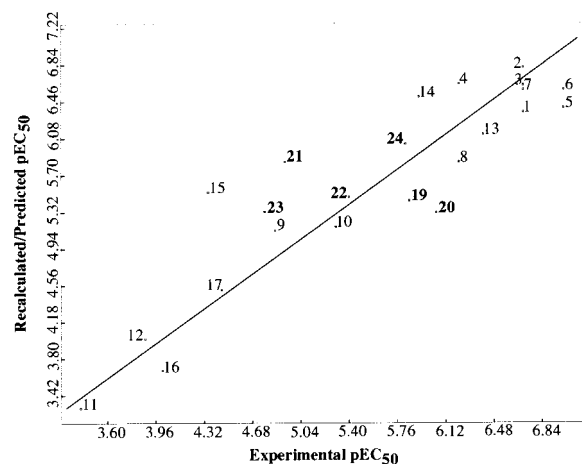


Figure 4. 3D QSAR: experimental/recalculated pEC₅₀ (plain text) and experimental/predicted pEC₅₀ (bold).

with the backbone of LYS103, PRO225, PRO226, PHE227, LEU234, HIS235, and PRO236.

Finally, the bound conformation of **1** was used, assuming a common binding mode, to model the other DAMNI derivatives (Table 1), which were subsequently evaluated by the NNRTI/VALIDATE II model.²² Although the absolute average error predicted by VALIDATE II model was only 0.49 pIC₅₀, it resulted from marginal statistical value when compared to the absolute average deviation (0.30 pIC₅₀). Anyway, the general numerical agreement between the experimental and recalculated activities for compounds **1**–**8** suggests that the synthesized compounds are likely to bind to RT NNBS, as evinced from the docking experiments.

3D QSAR. A three-dimensional quantitative structure–activity relationship (3D QSAR) was also carried out with the GRID and GOLPE programs to correlate the in vitro inhibitory activities (EC₅₀) with the structural variability of the test derivatives. The molecular alignment of the DAMNI derivatives was straightforward employing the minimized molecules inside the NNBS.

Since the overall structural variance of DAMNIs was focused only on the phenyl modeled into a hydrophobic aromatic pocket, we used the aromatic carbon atom probe for calculating the GRID molecular interaction fields.

All three-dimensional structure–activity relationships (3D SARs) have therefore been focused on the region surrounding the substituted phenyl ring, since all the other regions reflect features common to all the DAMNI derivatives. The structure–activity correlation was obtained using the GOLPE procedure. The GOLPE analysis, using the SRD algorithm, identified the significant GRID variables corresponding to the regions of the molecules involved in the binding to the HIV-1-RT. The PLS model, derived from the 308 variables selected from the starting 2448, was optimal with only two PLS components with the following associated statistical values of $r^2 = 0.87$, $q^2_{\text{LOO}} = 0.71$, and $\text{SDEP}_{\text{LOO}} = 0.64$ (Figure 4). Because satisfactory statistical parameters were achieved, we believe that the molecular alignment used provides further support to the previous suggested binding mode. The 3D QSAR model successfully recalculated the pEC₅₀ of previously

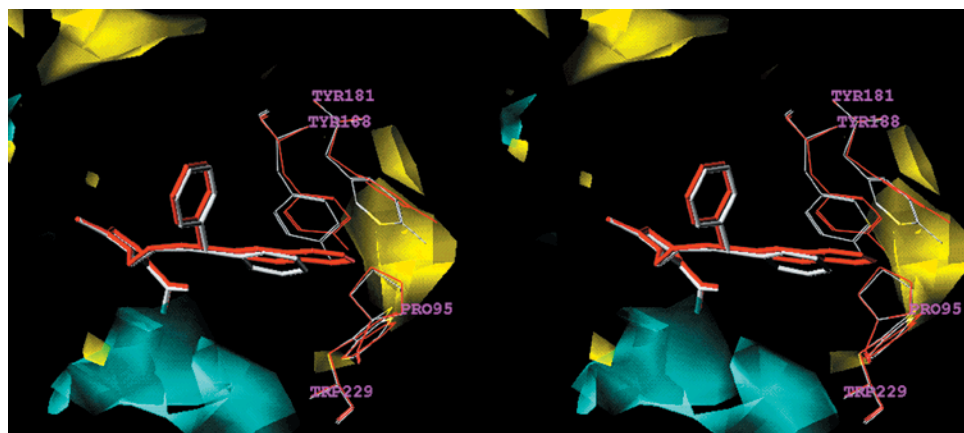


Figure 5. Stereoview of the GRID plot of PLS partial weights superimposed with the NNBS.

Table 3. Experimental and Recalculated pEC₅₀ of DAMNIs 19–24¹

compd	R ₁	R ₂	R ₃	R ₄	actual pEC ₅₀	predicted pEC ₅₀
19	H	H	CH ₃	H	5.85	5.44
20	H	H	F	H	6.05	5.32
21	H	H	Cl	H	4.92	5.84
22	H	H	<i>t</i> -butyl	H	5.40	5.47
23	H	H	phenyl	H	4.77	5.32
24	Cl	H	Cl	H	5.82	6.00

reported DAMNIs that were not included in the training set (SDEP = 0.56, Table 3).

The GRID plot of the partial weights (Figure 5) identifies areas in space that contribute most to the biological activity. Figure 5 highlights areas representing the regions of interaction between the target molecules and the GRID lattice nodes, and it includes as an example the structures of **1**, in white, and **17**, in red. Positive regions, in yellow, highlight areas where favorable interactions are correlated with a decrease of activity or where repulsive interactions are correlated with an increase of activity, while negative regions, in cyan, highlight areas where favorable interactions are correlated with an increase of activity or where repulsive interactions are correlated with a decrease of activity. The naphthyl group of **17** interacts with a positive region more than the phenyl group of **1**, thus explaining the weaker activity of **17**. For the same negative contribution, all the para-substituted DAMNIs were less potent than the lead compound **1**. Comparing this GRID region with the RT NNBS, it is possible to observe that the enzyme pocket in that area is fairly rigid, not allowing the suitable adjustment for bulkier moieties such as in compounds **10–12**, **16**, and **17**. In particular, a big yellow polyhedra (unfavorable interactions) is placed in almost the same 3D space occupied by the aromatic side chains of residues TYR181, TYR188, and TRP229. These three residues are fairly rigid (wall-resides). In fact, upon complex minimization, their side chain positions move very little, thus preventing a possible fitting of either a bulkier substituent in the para position of the DAMNIs or a bigger aromatic portion such as in compound **17** (Figure 5). Other big contours probably due to long-range interactions are also present: one in yellow corresponding to residues GLY190, SER191, and ASP192 and one in cyan (favorable interactions) corresponding to residues PRO97, LEU228, PHE227, TRP239, and TRY318. The absence

of GRID maps for the ortho- and meta-substituted DAMNIs can be explained by the fact that there is very little variance in the activities for these derivatives. In fact, the IC₅₀ of ortho and meta derivatives ranged from 0.1 (compounds **5** and **6**) to 0.6 (compound **8**).

The bulky nitro and pyrrole groups of compounds **8** and **9** approach the yellow contour and thus interact with wall residues, accounting for their decreased activity with respect to **1**. In a similar way, the disubstituted compounds **13–16** show steric hindrance of their substituents increasing inversely to their related IC₅₀ values.

Conclusions

We have recently described DAMNIs, a potent class of NNRTIs active at submicromolar concentrations. DAMNIs are characterized by a benzhydryloxy moiety, which mimics the “butterfly-like” conformation of the Schäfer 3D model, which is linked to the 2-methyl-5-nitroimidazole group through an ethylene bridge.

Attempts to increase the anti-HIV-1 activity by introducing substituents at one benzene ring of the benzhydryl moiety led to different results depending on the nature, position, and number of the atoms or groups introduced. High potency and low cytotoxicity were associated with the fluorine atom and the methyl group, especially when placed in the meta position. The meta-chloro analogue of **1** was also endowed with high activity and selectivity.

Introduction of two substituents in the phenyl ring furnished compounds with similar or less activity than the monosubstituted counterparts. Among disubstituted DAMNIs, 3,5-dimethyl and 3,5-difluoro derivatives were significantly more potent than the related 3,5-dichloro derivative.

Molecular modeling and docking inside the RT NNBS led us to conclude that DAMNIs, like some classical NNRTIs (nevirapine, TIBO, HEPT, α -APA, TBZ, and DABO), bind to reverse transcriptase assuming a “butterfly-like” orientation.¹ Moreover, DAMNIs bear a flexible tail [the 1-(2-methyl-5-nitroimidazolyl)ethyl group] that seems to behave like the 5-methanesulfonamidoindole-2-carbonylpiperazine portion of BHAP. Because of these features, DAMNIs are a hybrid class that mimics both the above classical NNRTIs and the BHAP derivatives.

From the docking studies, some insights for further lead optimization can be deduced. Considering the two

binding conformations of **1**, it is suggested that novel DAMNI derivatives bearing two hydrogen bond acceptors on the flexible tail could lead to more potent derivatives.

Experimental Section

Chemistry. Melting points (mp) were determined on a Büchi 510 apparatus and are uncorrected. Infrared spectra (IR) were run on a Perkin-Elmer 1310 spectrophotometer. Proton nuclear magnetic resonance ($^1\text{H NMR}$) spectra were recorded on a Bruker AM-200 (200 MHz) FT spectrometer in the indicated solvent. Chemical shifts are expressed in δ units (ppm) from tetramethylsilane. Standard abbreviations were used (s, d, t, q, dd, m, broad, u = unresolved). Column chromatographies were packed with silica gel Merck 60 (70–230 mesh). Fluka aluminum oxide/TLC cards (aluminum oxide precoated aluminum cards with fluorescent indicator at 254 nm), Fluka silica gel/TLC cards and Macherey-Nagel Alugram Sil G/UV₂₅₄ (silica gel precoated aluminum cards with fluorescent indicator at 254 nm) were used for thin-layer chromatography (TLC). Developed plates were visualized by a spectroline ENF 260C/F UV apparatus. Organic solutions were dried over anhydrous sodium sulfate. Concentration and evaporation of the solvent after reaction or extraction were carried out on a rotary evaporator (Büchi Rotavapor) operating at reduced pressure. Elemental analyses were performed by the laboratory of Dr. M. Zancato, Dipartimento di Scienze Farmaceutiche, University of Padova (Italy). Analytical results were within $\pm 0.4\%$ of the theoretical values.

General Procedure for the Synthesis of DAMNIs 2–4.

Example. 1-[2- α -(2-Methylphenyl)phenylmethoxy]ethyl]-2-methyl-5-nitroimidazole (2**).** A solution of phosphorus tribromide (3.12 g, 0.012 mol) in anhydrous diethyl ether (15 mL) was dropped into a well-stirred solution of 2-methylbenzhydrol (2.38 g, 0.012 mol) in the same solvent (60 mL). After being stirred at room temperature for 4 h, reaction mixture was quenched with 5% sodium acetate aqueous solution. The organic layer was separated, washed with brine, and dried. Removal of the solvent gave an oily residue that was used without further purification. A mixture of bromide (0.004 mol), 1-(2-hydroxyethyl)-2-methyl-5-nitroimidazole (0.68 g, 0.004 mol), K_2CO_3 (1.66 g, 0.012 mol), and acetone (40 mL) was refluxed for 7 days. After 24 and 48 h, 0.004 mol of bromide and 0.012 mol of K_2CO_3 were added. The mixture was diluted with water and extracted with ethyl acetate. Organic extracts were washed with brine and dried. Removal of the solvent gave a residue that was purified by silica gel column chromatography (chloroform as eluent) to give **2** (0.38 g, 27%), mp 97–99 °C (ligroin). $^1\text{H NMR}$ (CDCl_3): δ 2.28 (s, 3H), 2.57 (s, 3H), 3.75 (t, $J = 4.9$ Hz, 2H), 4.54 (t, $J = 4.9$ Hz, 2H), 5.22 (s, 1H), 6.88–7.30 (m, 9H), 7.96 (s, 1H). Anal. ($\text{C}_{20}\text{H}_{21}\text{N}_3\text{O}_3$) (351.40) C, H, N.

1-[2- α -(2-Fluorophenyl)phenylmethoxy]ethyl]-2-methyl-5-nitroimidazole (3**).** Yield 9%, mp 73–75 °C (ligroin). $^1\text{H NMR}$ (CDCl_3): δ 2.54 (s, 3H), 3.80 (m, 2H), 4.54 (m, 2H), 5.62 (s, 1H), 6.90–7.32 (9H), 7.94 ppm (s, 1H). Anal. ($\text{C}_{19}\text{H}_{18}\text{FN}_3\text{O}_3$) (355.37) C, H, N, F.

1-[2- α -(2-Chlorophenyl)phenylmethoxy]ethyl]-2-methyl-5-nitroimidazole (4**).** Yield 13%, mp 78 °C (ligroin). $^1\text{H NMR}$ (CDCl_3): δ 2.51 (s, 3H), 3.79 (u, 2H), 4.54 (u, 2H), 5.72 (s, 1H), 7.09–7.40 (m, 9H), 7.94 (s, 1H). Anal. ($\text{C}_{19}\text{H}_{18}\text{ClN}_3\text{O}_3$) (371.82) C, H, N, Cl.

General Procedure for the Synthesis of 5–18. Example. 1-[2- α -(3-Methylphenyl)phenylmethoxy]ethyl]-2-methyl-5-nitroimidazole (5**).** A mixture of the 3-methylbenzhydrol (1.98 g, 0.01 mol), 1-(2-hydroxyethyl)-2-methyl-5-nitroimidazole (0.46 g, 0.0027 mol), *p*-toluenesulfonic acid monohydrate (PTSA, 0.65 g, 0.0034 mol), and benzene (65 mL) was refluxed for 4 h. Water that formed during reaction was removed by azeotropic distillation by a Dean–Stark trap. After cooling, the reaction mixture was concentrated to a small volume and extracted with ethyl acetate. Combined organic extracts were washed with brine and dried. Evaporation of the

solvent afforded a crude product that was purified on a silica gel column chromatography (chloroform as eluent) to give **5** (0.35 g, 37%), mp 98–99 °C (ligroin). $^1\text{H NMR}$ (CDCl_3): δ 2.23 (s, 3H), 2.55 (s, 3H), 3.76 (u, 2H), 4.54 (u, 2H), 5.21 (s, 1H), 6.89–7.32 (m, 9H), 7.94 (s, 1H). Anal. ($\text{C}_{20}\text{H}_{21}\text{N}_3\text{O}_3$) (351.40) C, H, N.

1-[2- α -(3-Fluorophenyl)phenylmethoxy]ethyl]-2-methyl-5-nitroimidazole (6**).** Yield 54%, mp 121–123 °C (ligroin). $^1\text{H NMR}$ (CDCl_3): δ 2.55 (s, 3H), 3.77 (t, $J = 4.9$ Hz, 2H), 4.54 (t, $J = 4.9$ Hz, 2H), 5.23 (s, 1H), 6.80–6.97 (m, 3H), 7.06–7.15 (m, 2H), 7.17–7.31 (m, 4H), 7.94 (s, 1H). Anal. ($\text{C}_{19}\text{H}_{18}\text{FN}_3\text{O}_3$) (355.37) C, H, N, F.

1-[2- α -(3-Chlorophenyl)phenylmethoxy]ethyl]-2-methyl-5-nitroimidazole (7**).** Yield 67%, mp 99–101 °C (toluene/ligroin). $^1\text{H NMR}$ (CDCl_3): δ 2.54 (s, 3H), 3.75 (t, $J = 5.0$ Hz, 2H), 4.52 (t, $J = 5.0$ Hz, 2H), 5.21 (s, 1H), 6.92–7.35 (m, 9H), 7.93 (s, 1H). Anal. ($\text{C}_{19}\text{H}_{18}\text{ClN}_3\text{O}_3$) (371.82) C, H, N, Cl.

1-[2- α -(3-Nitrophenyl)phenylmethoxy]ethyl]-2-methyl-5-nitroimidazole (8**).** Yield 50%, thick oil. $^1\text{H NMR}$ (CDCl_3): δ 2.57 (s, 3H), 3.80 (t, $J = 5.0$ Hz, 2H), 4.58 (t, $J = 5.0$ Hz, 2H), 5.34 (s, 1H), 7.08–7.20 (m, 2H), 7.27–7.35 (m, 3H), 7.41–7.48 (m, 2H), 7.94 (s, 1H), 8.10 (m, 2H). Anal. ($\text{C}_{19}\text{H}_{18}\text{N}_4\text{O}_5$) (382.38) C, H, N.

1-[2- α -(3-(1*H*-Pyrrol-1-yl)phenyl)phenylmethoxy]ethyl]-2-methyl-5-nitroimidazole (9**).** Yield 28%, thick oil. $^1\text{H NMR}$ (CDCl_3): δ 2.56 (s, 3H), 3.80 (t, $J = 4.9$ Hz, 2H), 4.56 (t, $J = 4.9$ Hz, 2H), 5.28 (s, 1H), 6.33 (t, $J = 2.0$ Hz, 2H), 6.98–7.04 (m, 3H), 7.11–7.18 (m, 3H), 7.22–7.34 (m, 5H), 7.89 (s, 1H). Anal. ($\text{C}_{23}\text{H}_{22}\text{N}_4\text{O}_3$) (402.45) C, H, N.

1-[2- α -(4-Nitrophenyl)phenylmethoxy]ethyl]-2-methyl-5-nitroimidazole (10**).** Yield 36%, mp 115–118 °C (toluene/cyclohexane). $^1\text{H NMR}$ (CDCl_3): δ 2.54 (s, 3H), 3.80 (t, $J = 5.0$ Hz, 2H), 4.57 (t, $J = 5.0$ Hz, 2H), 5.34 (s, 1H), 7.04–7.14 (m, 2H), 7.23–7.38 (m, 5H), 7.93 (s, 1H), 8.14 (m, 2H). Anal. ($\text{C}_{19}\text{H}_{18}\text{N}_4\text{O}_5$) (382.38) C, H, N.

1-[2- α -(4-Acetamidophenyl)phenylmethoxy]ethyl]-2-methyl-5-nitroimidazole (11**).** Yield 36%, mp 115–118 °C (toluene/cyclohexane). $^1\text{H NMR}$ (CDCl_3): δ 2.14 (s, 3H), 2.54 (s, 3H), 3.75 (t, $J = 4.9$ Hz, 2H), 4.53 (t, $J = 4.9$ Hz, 2H), 5.22 (s, 1H), 7.02–7.14 (m, 4H), 7.17–7.30 (m, 4H, 3H after D_2O exchange), 7.33–7.44 (m, 2H), 7.94 (s, 1H). IR (Nujol): ν 1630, 3200 cm^{-1} . Anal. ($\text{C}_{21}\text{H}_{22}\text{N}_4\text{O}_4$) (394.43) C, H, N.

1-[2- α -(4-Methoxyphenyl)phenylmethoxy]ethyl]-2-methyl-5-nitroimidazole (12**).** Yield 76%, thick oil. $^1\text{H NMR}$ (CDCl_3): δ 2.54 (s, 3H), 3.68–3.80 (m, 5H), 4.52 (t, $J = 4.9$ Hz, 2H), 5.20 (s, 1H), 6.79 (d, $J = 8.6$ Hz, 2H), 6.98–7.15 (m, 4H), 7.18–7.28 (m, 3H), 7.93 (s, 1H). Anal. ($\text{C}_{20}\text{H}_{21}\text{N}_3\text{O}_4$) (367.40) C, H, N.

1-[2- α -(3,5-Dimethylphenyl)phenylmethoxy]ethyl]-2-methyl-5-nitroimidazole (13**).** Yield 32%, mp 112–113 °C (ligroin). $^1\text{H NMR}$ (CDCl_3): δ 2.24 (s, 6H), 2.55 (s, 3H), 3.75 (t, $J = 4.9$ Hz, 2H), 4.54 (t, $J = 4.9$ Hz, 2H), 5.17 (s, 1H), 6.70 (u, 2H), 6.84 (u, 1H), 7.06–7.16 (m, 2H), 7.20–7.32 (m, 3H), 7.94 (s, 1H). Anal. ($\text{C}_{21}\text{H}_{23}\text{N}_3\text{O}_3$) (365.43) C, H, N.

1-[2- α -(3,5-Difluorophenyl)phenylmethoxy]ethyl]-2-methyl-5-nitroimidazole (14**).** Yield 54%, mp 110–112 °C (ligroin). $^1\text{H NMR}$ (CDCl_3): δ 2.55 (s, 3H), 3.78 (m, 2H), 4.55 (t, $J = 5.0$ Hz, 2H), 5.20 (s, 1H), 6.60–6.70 (m, 3H), 7.02–7.16 (m, 2H), 7.22–7.33 (m, 3H), 7.95 (s, 1H). Anal. ($\text{C}_{19}\text{H}_{17}\text{F}_2\text{N}_3\text{O}_3$) (373.36) C, H, N, F.

1-[2- α -(3,5-Dichlorophenyl)phenylmethoxy]ethyl]-2-methyl-5-nitroimidazole (15**).** Yield 54%, mp 112–114 °C (diethyl ether). $^1\text{H NMR}$ (CDCl_3): δ 2.55 (s, 3H), 3.76 (t, $J = 5.0$ Hz, 2H), 4.55 (t, $J = 5.0$ Hz, 2H), 5.17 (s, 1H), 7.01 (m, 1H), 7.04–7.13 (m, 2H), 7.19–7.32 (m, 5H), 7.95 (s, 1H). Anal. ($\text{C}_{19}\text{H}_{17}\text{Cl}_2\text{N}_3\text{O}_3$) (406.27) C, H, N, Cl.

1-[2- α -(3,4-Dichlorophenyl)phenylmethoxy]ethyl]-2-methyl-5-nitroimidazole (16**).** Yield 18%, thick oil. $^1\text{H NMR}$ (CDCl_3): δ 2.54 (s, 3H), 3.76 (t, $J = 5.1$ Hz, 2H), 4.55 (t, $J = 5.1$ Hz, 2H), 5.20 (s, 1H), 6.95 (m, 1H), 7.03–7.13 (m, 2H), 7.21–7.38 (m, 5H), 7.95 (s, 1H). Anal. ($\text{C}_{19}\text{H}_{17}\text{Cl}_2\text{N}_3\text{O}_3$) (406.27) C, H, N, Cl.

1-[2- α -(Naphthalen-2-yl)phenylmethoxy]ethyl]-2-methyl-5-nitroimidazole (17**).** Yield 57%, thick oil. $^1\text{H NMR}$

(CDCl₃): δ 2.46 (s, 3H), 3.85 (m, 2H), 4.52 (m, 2H), 5.92 (s, 1H), 7.12–7.48 (m, 9H), 7.63–7.88 (m, 3H), 7.92 (s, 1H). Anal. (C₂₃H₂₁N₃O₃) (387.43) C, H, N.

1-[3-(Diphenylmethoxy)propyl]-2-methyl-5-nitroimidazole (18). Yield 78%, thick oil. ¹H NMR (CDCl₃): δ 2.07 (m, 2H), 2.43 (s, 3H), 3.48 (t, *J* = 5.5 Hz, 2H), 4.44 (t, *J* = 5.5 Hz, 2H), 5.31 (s, 1H), 7.18–7.37 (m, 10H), 7.92 (s, 1H). Anal. (C₂₀H₂₁N₃O₃) (351.40) C, H, N.

3-(1H-Pyrrol-1-yl)benzophenone (19). A solution of 3-aminobenzophenone (6.70 g, 0.034 mol) and 2,5-dimethoxytetrahydrofuran (90%, 9.00 g, 0.061 mol) in glacial acetic acid (100 mL) was refluxed for 1 h, then evaporated to dryness. After the mixture was shaken with ethyl acetate and water, the organic layer was separated, washed with brine, and dried. Removal of the solvent gave a residue that was passed through a silica gel column (chloroform as eluent) to give **19** (4.1 g, 49%), mp 79–81 °C (ligroin). ¹H NMR (CDCl₃): δ 6.37 (m, 2H), 7.13 (m, 2H), 7.32–7.68 (m, 6H), 7.78–7.87 (m, 3H). IR (Nujol): ν 1625 cm⁻¹. Anal. (C₁₇H₁₃NO) (247.29) C, H, N.

3-(1H-Pyrrol-1-yl)benzhydrol (20). Sodium borohydride (0.80 g, 0.021 mol) was added by portions to a solution of **19** (5.20 g, 0.021 mol) in THF (60 mL) containing 3.2 mL of water, and then the mixture was refluxed for 2 h. After it was cooled, water (40 mL) was added while stirring the mixture for a few minutes. After concentration to a small volume, the mixture was extracted with ethyl acetate, washed with brine, and dried. Removal of the solvent afforded pure **20** (5.2 g, 100%), mp 105–106 °C (ligroin). ¹H NMR (CDCl₃): δ 2.33 (br s, 1H, exchangeable with D₂O), 5.85 (s, 1H), 6.32 (m, 2H), 7.05 (m, 2H), 7.18–7.47 (m, 9H). IR (Nujol): ν 3390, 3430 cm⁻¹. Anal. (C₁₇H₁₅NO) (249.31) C, H, N.

4-Acetamidobenzophenone (21). Acetyl chloride (2.45 g, 0.030 mol) was dropped into an ice-cooled solution of 4-aminobenzophenone (6.00 g, 0.030 mol) in anhydrous pyridine (150 mL), and then the reaction was maintained at room temperature for 3 h. The mixture was diluted with water, made acidic with 37% aqueous HCl, and extracted with chloroform. The organic layer was washed with brine and dried. Evaporation of the solvent furnished a residue that was passed through a silica gel column (chloroform as eluent) to furnish **21** (6.0 g, 84%), mp 153–155 °C (toluene). ¹H NMR (CDCl₃): δ 2.22 (s, 3H), 7.42–7.70 (m, 5H), 7.72–7.86 (m, 4H). IR (Nujol): ν 1735 cm⁻¹. Lit.²⁴ mp 151–152 °C.

4-Acetamidobenzhydrol (22). **22** was prepared as **20** starting from **21**. Yield 90%, mp 138–140 °C (ligroin). ¹H NMR (CDCl₃): δ 2.15 (s, 3H), 2.32 (br s, 1H, exchangeable with D₂O), 5.81 (s, 1H), 7.20–7.49 (m, 9H). IR (Nujol): ν 1640, 3300, 3410, 3500 cm⁻¹. Anal. (C₁₅H₁₅NO₂) (241.29) C, H, N.

Molecular Modeling, Binding Mode Analysis, and 3D QSAR. Molecular modeling and 3D QSAR studies were performed with the software packages SYBYL 6.5,²⁵ MACROMODEL 6.5,²⁶ GRID 18,²⁷ and GOLPE 4.03²⁸ running on a Silicon Graphics O2 R10000 225 MHz. Field-fit minimizations were performed in SYBYL using the standard Tripos force field with an energy change convergence criterion of 0.001 kcal/mol. Charges were calculated using the GAST-HUCK/SYBYL module. Conformational analysis inside the NNBS and in water utilized MACROMODEL.

The structure of the DAMNI representative **1** was modeled from the isolated structure of TNK-651, extracted from the RT complex (PDB entry code 1rt2), using the SYBYL fragment library. The initial conformation for the docking experiments was achieved by a field-fit minimization of **1** using the steric and electrostatic fields of TNK-651 previously generated. A subsequent geometry optimization (100 iterations) without field fit of the aligned structure was performed to assign standard bond lengths and angles. The resulting initial structure of **1** showed a good overlapping of the two phenyl rings, with the aromatic moieties of the TNK-651 also displaying the methylnitroimidazolyl group in the same spatial region of the phenylmethoxy N-1 substituent. The same procedure conducted was repeated using as template the molecule delavirdine (BHAP U90192, PDB entry code 1klm). The field-fit routine superimposes a ligand upon another ligand

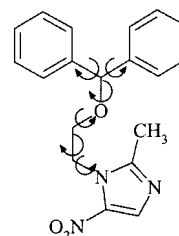


Figure 6. Rotatable bonds of **1**.

in order to maximize the similarity of their steric and electrostatic fields and then is strongly dependent on the initial input alignment. Therefore, we tried two further starting alignments by the use of the Monte Carlo/GBSA global minima of **1** superimposed on TNK and delavirdine through a feature-by-feature fit procedure (aromatic center to aromatic center, tail to tail, and hydrophobic center to hydrophobic center).

The geometry of the NNBS of HIV-1 RT was taken from the structure of HIV-1 RT/TNK-651. Residues within 20 Å from any ligand's atom (TNK-651), excluding all the water molecules present in the original PDB file, were used to define the NNBS.

The starting structure of the complex HIV-1 RT/**1** was obtained by replacing the TNK-651 with **1** inside the NNBS, as previously modeled and aligned from TNK-651. The docking of the DAMNI representative **1** was carried as follows. First, to investigate the NNBS flexibility, a SYBYL/FLEXIDOCK was performed with the default settings allowing the rotation of all the rotatable torsions of the ligand and the NNBS side chains torsions of all residues within 4 Å from the ligand. This docking experiment led to a binding conformation of **1** with an associated steric energy value of -270.885 kJ/mol (conformation a). Second, a Monte Carlo search was carried out with the MACROMODEL package (AMBER all atom force field). All the torsional bonds of **1** were rotated randomly while allowing them to relax within an 8 Å core of atoms of the NNBS during the minimization. An external fixed shell of 10 Å was also included for the long-range interactions. After 1000 Monte Carlo steps (MCM routine), in an energy window of 100 kJ/mol, 25 different local minima conformations were obtained. The global minimum that furnished a second binding conformation of **1** was found 11 times (conformation b, $E_{steric} = -260.617$ kJ/mol). Superimposition of all heavy atoms showed that conformations a and b were differing by a 1.8465 rmsd value. However, because the Monte Carlo search has the advantage of providing not just a global minimum but a range of possibilities and because the force field is not perfect, inspection of the molecular ensemble led to other local minima showing ligand conformations very similar to the binding conformation a. All four starting alignments mentioned above were routinely submitted to the search procedures without leading to substantially different results.

A further Monte Carlo search was also carried out in water (GB/SA solvation model²⁹) on all the rotatable torsionals (Figure 6) of the isolated modeled bound ligand using as the starting point either conformation a or conformation b. After 1000 Monte Carlo steps from the conformational searches, two isoenergetic global minima were obtained with a steric energy value of -295.29 kJ/mol, differing from each other by 1.0383 rmsd. Compared to the GB/SA global minima, the flexidocked conformation of **1** (conformation a) showed a strain energy value of 25.605 kJ/mol, while conformation b showed a value of 34.673 kJ/mol when compared with the two global minima conformations.

The ligand strain energy can be defined as the difference in steric energy (excluding the solvation term) between the bound and the global minimum of the free molecule as calculated using the GB/SA solvent model implemented in MACROMODEL.

$$\Delta E_{StrainEnergy} = E_{bound\ state} - E_{free\ state}$$

Minimization *in vacuo* of the isolated NNBS also led to

the computation of the receptor strain energies associated with the two binding modes (Table 2). Coulombic (electrostatic interaction energy, ESIE) and van der Waals (steric interaction energy, SIE) ligand–receptor interactions were obtained by the application of the VALIDATE code, in which electrostatic and steric complementarity is calculated using the explicit sum of the Coulombic and Lennard-Jones potentials.²¹

All other DAMNI compounds were modeled starting from conformation **1**, and since no information about their absolute active configurations was available, the structures were built by modifying the phenyl group closer to the more hydrophobic portion of NNBS, formed by the residues TYR181, TYR188, PHE227, TRP229, and LEU234. This procedure led us to model the DAMNIs in their *R* absolute configurations.

For the VALIDATE II model prediction and for the 3D QSAR, all tested derivatives were minimized inside the NNBS, allowing an 8 Å core of atoms of the NNBS to relax during the minimization. An external fixed shell of 10 Å was also included for the long-range interactions.

Upon minimization, the DAMNI-bound conformations were extracted from NNBS and directly used for the 3D QSAR. The GRID program was used to describe the superposed molecular structures. GRID is a computational procedure for detecting energetically favorable binding sites of molecules. The program calculates the interactions between the molecule and a probe atom that is moved through a regular grid of points in a region of interest around the target molecule. At each grid point, the interaction energy between the probe and the target molecule is calculated as the sum of Lennard-Jones, hydrogen bond, and electrostatic interactions. GRID contains a table of parameters to describe each type of atom occurring in each type of ligand molecules. These parameters define the strength of the Lennard-Jones, hydrogen bond, and electrostatic interactions made by an atom and are used to evaluate the energy functions. GRID probes are very specific in a way that they give precise spatial information, and their specificity and sensitivity are an advantage because the probes may be representative of the important chemical groups present in the active site, provided that the statistical method used for the analysis can distinguish between different types of interactions.

Since there is much experimental evidence of the 3D structure at the NNBS and most of the DAMNI structural variance is located on one of the phenyl groups that was modeled in the aromatic-rich portion of NNBS, we decided to use the aromatic carbon atom to mimic the above portion of the enzyme pocket. The energy calculations were performed using 2.0 Å spacing between the grid points. Each set of calculated interaction energies contained in the resulting 3D matrix, arranged as a one-dimensional vector, was used as input for the program GOLPE. The GRID variables matrix was correlated with the EC₅₀ in vitro activity by a PLS model using the GOLPE procedure. To obtain a model with better predictive capability, variable selection was operated by the application of the smart region definition (SRD) algorithm³⁰ with the following parameters: (i) 244 seeds (10% active variables) selected in the PLS weight space, (ii) critical distance cutoff of 2.5 Å, and (iii) collapsing distance cutoff of 4 Å. The SRD selected 23 boxes comprising 308 variables that were used without further variable selection. The model dimensionality chosen was that showing the best predictive ability and the active variables remaining after the SRD selection. Finally, a new PLS model was derived only on the basis of the active variables/regions.

The PLS model for the DAMNIs was obtained with molecules **1–17**. Molecule **18** was not included in the training set because no efforts were made to determine its putative binding-mode conformation.

An external test set compiled with previous reported DAMNIs⁶ was used to test the predictive capability of the 3D QSAR DAMNI model.

Antiviral Assay Procedures. Compounds. Compounds were solubilized in DMSO at 200 mM and then diluted into culture medium.

Cells and Viruses. MT-4, C8166, H9/III_B, and CEM cells were grown at 37 °C in a 5% CO₂ atmosphere in RPMI 1640 medium, supplemented with 10% fetal calf serum (FCS), 100 IU/mL penicillin G and 100 µg/mL streptomycin. Cell cultures were checked periodically for the absence of mycoplasma contamination with a MycoTect Kit (Gibco). Human immunodeficiency viruses type 1 (HIV-1, III_B strain) and type 2 (HIV-2 ROD strain, kindly provided by Dr. L. Montagnier, Paris) were obtained from supernatants of persistently infected H9/III_B and CEM cells, respectively. HIV-1 and HIV-2 stock solutions had titers of 4.5×10^6 and 1.4×10^5 50% cell culture infectious dose (CCID₅₀) per milliliter, respectively.

HIV Titration. Titration of HIV was performed in C8166 cells with the standard limiting dilution method (dilution 1:2, four replica wells per dilution) in 96-well plates. The infectious virus titer was determined by light microscope scoring of cytopathicity after 4 days of incubation, and the virus titers were expressed as CCID₅₀/mL.

Anti-HIV Assays. Evaluation of the activity of the compounds against HIV-1 and HIV-2 replication in acutely infected cells was based on the inhibition of virus-induced cytopathicity in MT-4 and C8166 cells, respectively. Briefly, a total of 50 µL of culture medium containing 1×10^4 cells was added to each well of flat-bottom microtiter trays containing 50 µL of culture medium with or without various concentrations of the test compounds. Then a total of 20 µL of an HIV suspension containing 100 (HIV-1) or 1000 (HIV-2) CCID₅₀ (50% cell culture infective dose) was added. After a 4-day incubation (5 days for HIV-2) at 37 °C, the number of viable cells was determined by the 3-(4,5-dimethylthiazol-1-yl)-2,5-diphenyltetrazolium bromide (MTT) method.³¹ Cytotoxicity of the compounds was evaluated in parallel with their antiviral activity. It was based on the viability of mock-infected cells, as monitored by the MTT method.

RT Assays. Assays were performed as previously described.³² Briefly, purified rRT was assayed for its RNA-dependent polymerase-associated activity in a 50 µL volume containing 50 mM Tris-HCl (pH 7.8), 80 mM KCl, 6 mM MgCl₂, 1 mM DTT, 0.1 mg mL⁻¹ BSA, 0.5 OD₂₆₀ unit per milliliter template/primer [poly(rC)/oligo(dG)_{12–18}], and 10 mM [³H]dGTP (1 Ci mmol⁻¹). After incubation for 30 min at 37 °C, the samples were spotted on glass fiber filters (Whatman GF/A) and the acid-insoluble radioactivity was determined.

Acknowledgment. Authors thank the Italian Ministero della Sanità—Istituto Superiore di Sanità—IX Progetto AIDS 1996 (Grant Nos. 40A.0.06 and 9403-59) for financial aid. Acknowledgments are also due to the Italian MURST (40% funds) and Regione Autonoma Sardegna (Assessorato Sanità) for partial support. Thanks are due to Prof. G. R. Marshall for a critical review of the manuscript.

References

- (1) Schäfer, W.; Friebe, W.-G.; Leinert, H.; Mertens, H.; Poll, T.; von der Saal, W.; Zilch, H.; Nuber, B.; Ziegler, M. L. Non nucleoside inhibitors of HIV-1 reverse transcriptase: molecular modeling and X-ray structure investigations. *J. Med. Chem.* **1993**, *36*, 726–732.
- (2) Schäfer, W. Rational design of inhibitors of HIV-1 reverse transcriptase. In *Methods and principles in medicinal chemistry. Structure-based ligand design*; Gubernator, K., Böhm, H.-J., Eds.; Wiley-VCH: Weinheim, Germany, 1998.
- (3) (a) Artico, M.; Massa, S.; Mai, A.; Marongiu, M. E.; Piras, G.; Tramontano, E.; La Colla, P. 3,4-Dihydro-2-alkoxy-6-benzyl-4-oxopyrimidines (DABOs), a new class of specific inhibitors of human immunodeficiency virus type 1. *Antiviral Chem. Chemother.* **1993**, *4*, 361–368. (b) Mai, A.; Artico, M.; Sbardella, G.; Massa, S.; Novellino, E.; Greco, G.; Loi, A. G.; Tramontano, E.; Marongiu, M. E.; La Colla, P. 5-Alkyl-2-(alkylthio)-6-(2,6-dihalophenylmethyl)-3,4-dihydropyrimidin-4(3H)-ones: Novel Potent and Selective Dihydro-alkoxy-benzyl-oxopyrimidine Derivatives. *J. Med. Chem.* **1999**, *42*, 619–627.
- (4) Pauwels, R.; Andries, K.; Debyser, Z.; Van Daele, P.; Schols, D.; Stoffels, P.; De Vreese, K.; Woestenborghs, R.; Vandamme, A.-M.; Janssen, C. G. M.; Anne, J.; Cauwenbergh, G.; Desmyter,

- J.; Heykants, J.; Janssen, M. A. C.; De Clercq, E.; Janssen, P. A. J. Potent and highly selective human immunodeficiency virus type 1 (HIV-1) inhibition by a series of α -anilino-phenylacetamide derivatives targeted at HIV-1 reverse transcriptase. *Proc. Natl. Acad. Sci. U.S.A.* **1993**, *90*, 1711–1715.
- (5) Chimirri, A.; Grasso, S.; Molica, C.; Monforte, A.-M.; Monforte, P.; Zappalà, M.; Bruno, G.; Nicolo, F.; Witvrouw, M.; Jonckere, H.; Balzarini, J.; De Clercq, E. Structural features and anti-human immunodeficiency virus (HIV) activity of the isomers of 1-(2',6'-difluorophenyl)-1*H*,3*H*-thiazolo[3,4-*a*]benzimidazole, a potent non nucleoside HIV-1 reverse transcriptase inhibitor. *Antiviral Chem. Chemother.* **1997**, *8*, 363–370.
- (6) Silvestri, R.; Artico, M.; Massa, S.; Marceddu, T.; De Montis, F.; La Colla, P. 1-[2-(Diphenylmethoxy)ethyl]-2-methyl-5-nitroimidazole: a potent lead for the design of novel NNRTIs. *Bioorg. Med. Chem. Lett.* **2000**, *10*, 253–256.
- (7) Cosar, P. C.; Crisan, C.; Horclois, R.; Jacob, R. M.; Robert, J.; Tchelitcheff, S.; Vaupré, R. Nitro-imidazoles—Préparation et activité chimiothéputique. *Arzneim.-Forsch.* **1966**, *16*, 23–29.
- (8) Montagne, M. P. S. De l'action d'une solution alcoolique des potasse caustique sur les cétones. *Recl. Trav. Chim. Pays-Bas* **1916**, *36*, 258–270.
- (9) (a) Clauson-Kaas, N.; Tyle, Z. Preparation of *Cis*- and *Trans*-2,5-Dimethoxy-2-(acetamidomethyl)tetrahydrofuran and 1-Phenyl-2-(acetamidomethyl)pyrrole. *Acta Chem. Scand.* **1952**, *6*, 667–670. (b) Elming, N.; Clauson-Kaas, N. The Preparation of Pyrroles from Furans. *Acta Chem. Scand.* **1952**, *6*, 867–874.
- (10) Massa, S.; Stefancich, G.; Corelli, F.; Silvestri, R.; Panico, S.; Artico, M.; Simonetti, N. Research on antibacterial and antifungal agents. IX. Pyrrole analogues of bifonazole with potent antifungal activities. *Farmaco, Ed. Sci.* **1988**, *43*, 693–704.
- (11) Tanaka, H.; Takashima, H.; Ubasawa, H.; Sekiya, K.; Nitta, I.; Baba, M.; Shigeta, S.; Walker, R. T.; De Clercq, E.; Miyasaka, T. Structure–activity relationships of 1-[(2-hydroxyethoxy)methyl]-6-(phenylthio)thymine analogues: effect of the substitution at C-6 phenyl ring and at C-5 position on anti-HIV-1 activity. *J. Med. Chem.* **1992**, *35*, 337–345.
- (12) Fujiwara, T.; Sato, A.; El-Farrash, M.; Miki, S.; Abe, K.; Isaka, Y.; Kodama, M.; Wu, Y.; Chen, B. L.; Harada, H.; Sugimoto, H.; Hatanaka, M.; Hinuma, Y. S-1153 inhibits replication of known drug-resistant strains of human immunodeficiency virus type 1. *Antiviral Chem. Chemother.* **1998**, *42*, 1340–1345.
- (13) Hopkins, A. L.; Ren, J.; Esnouf, R. M.; Willcox, B. E.; Jones, E. Y.; Ross, C.; Miyasaka, T.; Walker, R. T.; Tanaka, H.; Stammers, D. K.; Stuart, D. I. Complexes of HIV-1 reverse transcriptase inhibitors of the HEPT series reveal conformational changes to the design of potent non-nucleoside inhibitors. *J. Med. Chem.* **1996**, *39*, 1589–1600.
- (14) Romero, D. L.; Morge, R. A.; Genin, M. J.; Biles, C.; Busso, M.; Resnick, L.; Althaus, I. W.; Reusser, F.; Thomas, R. C.; Tarpley, W. G. Bis(heteroary)l)piperazine BHAP reverse transcriptase inhibitors: structure–activity relationships of novel substituted indole analogues and the identification of 1-[(5-methanesulfonamido-1*H*-indol-2-yl)-carbonyl]-4-[3-[(1-methylethyl)amino]pyridyl]-piperazine monomethanesulfonate (U-90152S), a second generation clinical candidate. *J. Med. Chem.* **1993**, *36*, 1505–1508.
- (15) Esnouf, R.; Ren, J.; Hopkins, A. L.; Ross, C. K.; Jones, E. Y.; Stammers, D. K.; Stuart, D. I. Unique features in the structure of the complex between HIV-1 reverse transcriptase and the bis-(heteroary)l)piperazine (BHAP) U90152 explain resistance mutations for this non nucleoside inhibitor. *Proc. Natl. Acad. Sci. U.S.A.* **1997**, *94*, 3984–3989.
- (16) Marshall, G. R.; Head, R. D.; Ragno, R. In *Thermodynamics in Biology*; di Cera, Enrico, Ed.; Oxford University Press, in press.
- (17) Ragno, R.; Head, R.; Marshall, G. A predictive model for HIV protease inhibitors. Presented at the 216th National Meeting of the American Chemical Society, 1998; Paper COMP 032.
- (18) Silvestri, R.; Artico, M.; De Martino, G.; Ragno, R.; Massa, S.; Serra, I.; Demontis, F.; Brunatte, G.; Doratiotto, S.; La Colla, P. Synthesis, anti-HIV-1 RT activity and binding mode of 1-[2-(diarylmethoxy)ethyl]-2-methyl-5-nitroimidazoles (DAMNIs). Presented at the XVth International Symposium on Medicinal Chemistry, 2000; Paper PC-153.
- (19) Quaglia, M.; Mai, A.; Sbardella, G.; Artico, M.; Ragno, R.; et al. Chiral resolution and molecular modeling investigation of rac-2-cyclopentylthio-6-[1-(2,6-difluorophenyl)ethyl]-3,4-dihydro-5-methylpyrimidin-4(3*H*)-one (MC-1047), a potent anti-HIV-1 reverse transcriptase agent of the DABO class. *Chirality* **2001**, *13*, 75–80 and references cited herein.
- (20) Boström, J.; Norrby, P. O.; Liljefors, T. Conformational energy penalties of protein-bound ligands. *J. Comput.-Aided Mol. Des.* **1998**, *12*, 383–396.
- (21) Head, R. D.; Smythe, M. L.; Oprea, T. I.; Waller, C. L.; Green, S. M.; Marshall, G. R. VALIDATE: a new method for the receptor-based prediction of binding affinity of novel ligands. *J. Am. Chem. Soc.* **1996**, *118*, 3959–3969.
- (22) Details on the HIV-RT/VALIDATE II model will be published elsewhere. Briefly, a quantitative hybrid QSAR/scoring function model was obtained using 14 experimental HIV-1 RT/inhibitor complexes (PDB entry codes: 1bqm, 1hni, 1hmv, 1klm, 1rt1, 1rt2, 1rth, 1tvr, 1vrt, 1rt4, 1rt5, 1rt6, and 1rt7) and 8 selected parameter/scores yielding $r^2 = 0.80$, $q^2_{\text{LOO}} = 0.59$, SDEP_{LOO} = 0.56 using 2 principal pls components.}
- (23) Mattos, C.; Ringe, D. Multiple Binding Modes. In *3D QSAR in Drug Design. Theory, Methods and Applications*; Kubunyi, H., Ed.; ESCOM: Leiden, The Netherlands, 1993; pp 117–136.
- (24) Peet, N. P.; Sunder, S.; Barbuch, R. J.; Whalon, M. R.; Huber, E. W.; Huffman, J. Reinvestigation of a 5*H*-dibenzo[*d,h*][1,3,6]triazinone synthesis. *J. Heterocycl. Chem.* **1989**, *26*, 1611–1618.
- (25) SYBYL Molecular Modeling System, version 6.5; Tripos Associated: St. Louis, MO.
- (26) Mohamadi, F.; Richards, N. G. J.; Guida, W. C.; Liskamp, R.; Lipton, M.; Caufield, C.; Chang, G.; Hendrickson, T.; Still, W. C. MACROMODEL, an Integrated Software System for Modeling Organic and Bioorganic Molecules Using Molecular Mechanics. *J. Comput. Chem.* **1990**, *11*, 440–467.
- (27) (a) Goodford, P. J. A computational procedure for determining energetically favorable binding sites on biologically important macromolecules. *J. Med. Chem.* **1985**, *28*, 849–857. (b) Wade, R. C.; Clark, K. J.; Goodford, P. J. Further development of hydrogen bond conditions for use in determining energetically favorable binding sites on molecules of known structure. 1. Ligand probe groups with the ability to form two hydrogen bonds. *J. Med. Chem.* **1993**, *36*, 140–147.
- (28) Baroni, M.; Costantino, G.; Cruciani, G.; Riganelli, D.; Valigi, R.; et al. Generating optimal linear PLS estimations (GOLPE): An advanced chemometric tool for handling 3D-QSAR problems. *Quant. Struct.–Act. Relat.* **1993**, *12*, 9–20.
- (29) Still, W. C.; Tempczyk, A.; Hawley, R. C.; Hendrickson, T. Semianalytical Treatment of Solvation for Molecular Mechanics and Dynamics. *J. Am. Chem. Soc.* **1990**, *112*, 6127–6129.
- (30) Pastor, M.; Cruciani, G.; Clementi, S. Smart region definition: a new way to improve the predictive ability and interpretability of three-dimensional quantitative structure–activity relationships. *J. Med. Chem.* **1997**, *40*, 1455–1464.
- (31) Pauwels, R.; Balzarini, J.; Baba, M.; Snoeck, R.; Schols, D.; Herdewijn, P.; Desmyter, J.; De Clercq, E. A rapid and automated tetrazolium-based colorimetric assay for the detection of anti HIV compounds. *J. Virol. Methods* **1988**, *20*, 309–321.
- (32) Tramontano, E.; Cheng, Y.-C. HIV-1 reverse transcriptase inhibition by a dipyrroliodiazepinone derivative: BI-RG-587. *Biochem. Pharmacol.* **1992**, *43*, 1371–1376.

JM010904A